Nik Mohd Izual bin Nik Ibrahim / FKM

Lattice Boltzmann Numerical Prediction of Natural Convection Heat Transfer in an Inclined Square Enclosure

C. S. N. Azwadi*and N. I. N. Ibrahim

Thermofluid Department, Faculty of Mechanical Engineering, Universiti Teknologi Malaysia, 81310 UTM Skudai, Johor, MALAYSIA
Thermofluid Department, Faculty of Mechanical Engineering, Universiti MalaysiaPahang, Pahang, MALAYSIA

SUMMARY

In this paper, a numerical method was applied to solve two dimensional, incompressible, thermal fluid flow problem. This study presents numerical prediction of free convection heat transfer inside an inclined square cavity with perfectly conducting boundary conditions for the top and bottom walls. The mesoscale lattice Boltzmann scheme with uniform mesh resolution was applied as a numerical research tool. The inclination angels were varied from 20^0 to 160^0 with 20^0 intervals. The results were presented in terms of streamlines, isotherms plots and average Nusselt number in the system. We found that the flow structure together with the heat transfer mechanism are significantly dependence on the magnitude of the inclination angles. Good agreements were obtained when compared with the results published by other researchers in previous studies. Copyright © 2000 John Wiley & Sons, Ltd.

KEY WORDS: Convection heat transfer, inclined enclosure, lattice Boltzmann method.

1. INTRODUCTION

Flow in an enclosure driven by buoyancy force is a fundamental problem in fluid mechanics. This type of flow is encountered in certain engineering applications within electronic cooling technologies, in everyday situation such as roof ventilation or in academic research where it may be used as a benchmark problem for testing newly developed numerical methods. A classic example is the case where the flow is induced by differentially heated walls of the cavity boundaries. Two vertical walls with constant hot and cold temperature is the most well defined geometry and was studied extensively in the literature. A comprehensive review was presented by Davis[1]. Other examples are the work by Azwadi and Tanahashi[2] and Tric[3].

The analysis of flow and heat transfer in a differentially heated side walls was extended to the inclusion of the inclination of the enclosure to the direction of gravity by Rasoul and Prinos[4]. This study performed numerical investigations in two dimensional thermal fluid flows which are induced by the buoyancy force when the two facing sides of the cavity are heated to different temperatures. The cavity was inclined at angles from 20^0 to 160^0, Rayleigh numbers from 10^3 to 10^6 and Prandtl numbers from 0.02 to 4000. Their results indicated that the mean and local heat flux at the hot wall were significantly depend on the inclination angle. They also found that this dependence becomes stronger for the inclination angle greater than 90^0.

Hart[5] performed a theoretical and experimental study of thermal fluid flow in a rectangular cavity at small aspect ratio and investigated the stability of the flow inside the system. Ozoe *et al.*[6] conducted numerical analysis using finite different method of two-dimensional natural circulation in four types of rectangular cavity at inclination angles from 0^0 to 180^0. Kuyper *et al.*[7] provided a wide range of numerical predictions of flow in an inclined square cavity, covered from laminar to turbulent regions of the flow behavior. They applied k-ϵ turbulence model and performed detailed analysis for Rayleigh numbers of 10^6 to 10^{10}.

A thorough search of the literature has revealed that no work has been reported for free convection in an inclined square cavity with Neumann typed of boundary conditions. The type of boundary condition applied on the bottom and top boundaries of the cavity strongly affects the heat transfer mechanism in the system[8]. Therefore, it is the purpose of present study to investigate the fluid flow behavior and heat transfer mechanism in an inclined square cavity, differentially heated sidewalls and perfectly conducting boundary condition for top and bottom walls.

The current study is summarized as follow: two dimensional fluid flow and heat transfer in an inclined square cavity is investigated numerically. The two sidewalls are maintained at different temperatures while the top and bottom walls are set as a perfectly conducting wall. In current study, we fix the aspect ratio to unity. The flow structures and heat transfer mechanism are highly dependent upon the inclination angle of the cavity. By also adopting the Rayleigh number as a continuation parameter, the flow structure and heat transfers mechanism represented by the streamlines and isotherms lines can be identified as function of inclination angle. The computed average Nusselt number is also plotted to demonstrate the effect of inclination angle on the thermal behaviour in the system. Section two of this paper presents the governing equations for the case study in hand and introduces the numerical method which will be adopted for its solution. Meanwhile section three presents the computed results and provides a detailed discussion. The final section of this paper concludes the current study.

2. NUMERICAL FORMULATION

In present research, the incompressible viscous fluid flow and heat transfer are studied in a differentially heated side walls and perfectly conducting boundary conditions for top and bottom walls. Then the square enclosure is inclined from 20^0 to 160^0 to investigate the effect of inclination angles on thermal and fluid flow characteristics in the system. The governing equations are solve indirectly: i. e. using the lattice Boltzmann mesoscale method (LBM) with second order accuracy in space and time.

Our literature study found that there were several investigations have been conducted using the LBM to understand the phenomenon of free convection in an enclosure[9][10][11].

However, most of them considered an enclosure at 90^0 inclination angle and adiabatic boundary conditions at top and bottom walls. To the best of authors' knowledge, only Lallemand *et al.*[12] predicted the natural convection in an inclined enclosure at two Rayleigh numbers and two aspect ratios. In their study, they investigated the fluid flow and heat transfer when an inclined partition is attached to the hot wall enclosure and assumed adiabatic boundary condition at the top and bottom walls. Due to lack of knowledge on the problem in hand, therefore, the objective of present paper is to gain better understanding for the current case study by using the lattice Boltzmann numerical method. To see this, we start with the evolution equations of the density and temperature distribution functions, given as[13]

$$f_i\left(\mathbf{x}+\mathbf{c}_i\Delta\mathbf{x}, t+\Delta t\right) - f_i\left(\mathbf{x}, t\right) = -\frac{1}{\tau_v}\left(f_i\left(\mathbf{x}, t\right) - f_i^{eq}\left(\mathbf{x}, t\right)\right) + F_i \tag{1}$$

$$g_i\left(\mathbf{x}+\mathbf{c}_i\Delta\mathbf{x}, t+\Delta t\right) - g_i\left(\mathbf{x}, t\right) = -\frac{1}{\tau_c}\left(g_i\left(\mathbf{x}, t\right) - g_i^{eq}\left(\mathbf{x}, t\right)\right) \tag{2}$$

where the density distribution function $f = f\left(\mathbf{x}, t\right)$ is used to calculate the density and velocity fields and the temperature distribution function $g = g\left(\mathbf{x}, t\right)$ is used to calculate the macroscopic temperature field. Note that Bhatnagar-Gross-Krook (BGK) collision model[14] with a single relaxation time is used for the collision term. For the D2Q9 model (two-dimension nine-lattice velocity model), the discrete lattice velocities are defined by

$$\begin{aligned} \mathbf{c}_0 &= (0,0) \\ \mathbf{c}_i &= c\left(\cos\left(\left(i-1\right)\pi/2\right), \sin\left(\left(i-1\right)\pi/2\right)\right), i = 1-4 \\ \mathbf{c}_i &= \sqrt{2}c\left(\cos\left(\left(i-5\right)\pi/2+\pi/4\right), \sin\left(\left(i-5\right)\pi/2+\pi/4\right)\right), i = 5-8 \end{aligned} \tag{3}$$

Here, c is the lattice spacing. In LBM, the magnitude of $\mathbf{c}_i$ is set up so that in each time step Δt, the distribution function propagates in a distance of lattice nodes spacing Δx. This will ensure that the distribution function arrives exactly at the lattice nodes after Δt. The equilibrium function for the density distribution function f_i^{eq} for the D2Q9 model is given by

$$f_i^{eq} = \rho\omega_i\left[1 + 3\mathbf{c}_i\cdot\mathbf{u} + \frac{9\left(\mathbf{c}_i\cdot\mathbf{u}\right)^2}{2} - \frac{3\mathbf{u}^2}{2}\right] \tag{4}$$

where the weights are $\omega_0 = \frac{4}{9}$, $\omega_i = \frac{1}{9}$ for $i = 1-4$ and $\omega_i = \frac{1}{36}$ for $i = 5-8$.

According to Azwadi and Tanahashi[8] and Hou *et al.*[13], the expression for equilibrium function of temperature distribution can be written as

$$\begin{aligned} g^{eq} &= \rho T\left(\frac{1}{2\pi RT}\right)^{D/2} exp\left\{-\frac{\mathbf{c}^2}{2RT}\right\}\left[\frac{\mathbf{c}^2}{DRT} + \left(\frac{\mathbf{c}^2}{DRT} - \frac{2}{D}\right)\frac{\mathbf{c}\cdot\mathbf{u}}{RT}\right. \\ &\quad \left. + \left(\frac{\mathbf{c}^2}{DRT} - \frac{4}{D}\right)\frac{\left(\mathbf{c}\cdot\mathbf{u}\right)^2}{2(RT)^2} - \left(\frac{\mathbf{c}^2}{DRT} - \frac{2}{D}\right)\frac{\mathbf{u}^2}{2RT}\right]. \end{aligned} \tag{5}$$

Regroup Eq. (5) to avoid higher order quadrature gives

$$\begin{aligned} g^{eq} &= \rho T\left(\frac{1}{2\pi RT}\right)^{D/2} exp\left\{-\frac{\mathbf{c}^2}{2RT}\right\}\left[1+\frac{\mathbf{c}\cdot\mathbf{u}}{RT}+\frac{(\mathbf{c}\cdot\mathbf{u})^2}{2(RT)^2}-\frac{\mathbf{u}^2}{2RT}\right]+ \\ &\quad \rho T\left(\frac{1}{2\pi RT}\right)^{D/2} exp\left\{-\frac{\mathbf{c}^2}{2RT}\right\}\left[\frac{\mathbf{c}^2}{DRT}-1\right]+ \\ &\quad \rho T\left(\frac{1}{2\pi RT}\right)^{D/2} exp\left\{-\frac{\mathbf{c}^2}{2RT}\right\}\left[\left(\frac{\mathbf{c}^2}{DRT}-\frac{2+D}{D}\right)\frac{\mathbf{c}\cdot\mathbf{u}}{RT}+\right. \\ &\quad \left.\left(\frac{\mathbf{c}^2}{DRT}-\frac{4+D}{D}\right)\frac{(\mathbf{c}\cdot\mathbf{u})^2}{2(RT)^2}-\left(\frac{\mathbf{c}^2}{DRT}-\frac{2+D}{D}\right)\frac{\mathbf{u}^2}{2RT}\right]. \end{aligned} \tag{6}$$

It has been proved by Guo[15] that the zeroth through second order moments in the last square bracket and the zeroth and first order moments in the second square bracket in the right hand side of Eq. (6) vanish. The exclusion of the second order moments in the second square bracket in Eq. (6) only related to the constant parameter in the thermal conductivity which can be absorbed by manipulating the parameter τ_c in the computation. Therefore, by dropping the terms in the last two square brackets on the right hand side of Eq. (6) gives

$$g^{eq} = \rho T\left(\frac{1}{2\pi RT}\right)^{D/2} exp\left\{-\frac{\mathbf{c}^2}{2RT}\right\}\left[1+\frac{\mathbf{c}\cdot\mathbf{u}}{RT}+\frac{(\mathbf{c}\cdot\mathbf{u})^2}{2(RT)^2}-\frac{\mathbf{u}^2}{2RT}\right]. \tag{7}$$

After some modifications in order to satisfy the macroscopic energy equation via the Chapmann-Enskog expansion procedure, the discretised equilibrium function for the temperature distribution can be expressed as

$$g_i^{eq} = T\omega_i\left[1+3\mathbf{c}_i\cdot\mathbf{u}+\frac{9\left(\mathbf{c}_i\cdot\mathbf{u}\right)^2}{2}-\frac{3\mathbf{u}^2}{2}\right] \tag{8}$$

where the weights are $\omega_0=\frac{4}{9}$, $\omega_i=\frac{1}{9}$ for $i=1-4$ and $\omega_i=\frac{1}{36}$ for $i=5-8$. The macroscopic variables, density ρ, and temperature T can thus be evaluated as the moment to the equilibrium distribution functions as

$$\rho=\sum\nolimits_i f_i^{eq}, T=\sum\nolimits_i g_i^{eq} \tag{9}$$

Through a multiscaling expansion, the mass and momentum equations can be derived for D2Q9 model. The detail derivation of this is given by Luo *et al.*[16] and will not be shown here. The kinematic viscosity of fluid is given by

$$\nu=\frac{2\tau_v-1}{6}. \tag{10}$$

The energy equation at the macroscopic level can be expressed as follow

$$\frac{\partial}{\partial t}\rho T+\nabla\cdot\rho\mathbf{u}T=\chi\nabla^2\left(\rho T\right). \tag{11}$$

where χ is the thermal diffusivity. Thermal diffusivity and the relaxation time of temperature distribution function is related as

$$\chi=\frac{2\tau_c-1}{6}. \tag{12}$$

3. PROBLEM PHYSICS AND NUMERICAL RESULTS

The physical domain of the problem is represented in Fig. 1. The conventional no-slip boundary conditions[17] are imposed on all the walls of the cavity. The thermal conditions applied on the left and right walls are $T(x=0,y)=T_H$ and $T(x=L,y)=T_C$. The top and bottom walls being perfectly conducted, $T=T_H-\left(\frac{x}{L}\right)(T_H-T_C)$, where T_H and T_C are hot and cold temperature, and L is the width of the enclosure. The temperature difference between the left and right walls introduces a temperature gradient in a fluid, and the consequent density difference induces a fluid motion, that is, convection.

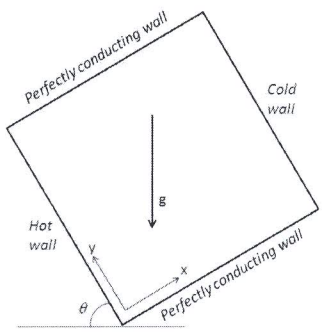

Figure 1. Physical domain of the problem.

The Boussinesq approximation is applied to the buoyancy force term. With this approximation, it is assumed that all fluid properties can be considered as constant in the body force term except for the temperature dependence of the density in the gravity term. So the external force in Eq. (1) is

$$F_i = 3\mathbf{G}\left(\mathbf{c}-\mathbf{u}\right)f_i^{eq} \tag{13}$$

where $\mathbf{G}$ is the contribution from buoyancy force.

The dynamical similarity depends on two dimensionless parameters: the Prandtl number Pr and the Rayleigh number Ra,

$$Pr=\frac{\nu}{\chi}, Ra=\frac{g_0\beta\Delta TL^3}{\nu\chi}. \tag{14}$$

We carefully choose the characteristic speed $v_c=\sqrt{g_0LT}$ so that the low-Mach-number approximation is hold. Nusselt number, Nu is one of the most inportant dimensionless numbers in describing the convective transport. The average Nusselt number in the system is defined by

$$Nu=\frac{H}{\chi\Delta T}\frac{1}{H^2}\int_0^H\int_0^H q_x\left(x,y\right)dxdy \tag{15}$$

where $q_x\left(x,y\right)=uT\left(x,y\right)-\chi\left(\partial/\partial x\right)T\left(x,y\right)$ is the local heat flux in $x-$direction.

In all simulations, Pr is set to be 7.0 to represent the circulation of water in the system. Through the grid dependence study, the grid sizes of 251×251 is suitable for Rayleigh numbers

from 10^5 to 10^6. The convergence criterion for all the tested cases is

$$\text{Max}\left|\left(\left(u^2+v^2\right)^{n+1}\right)^{\frac{1}{2}}-\left(\left(u^2+v^2\right)^{n}\right)^{\frac{1}{2}}\right|\leq 10^{-7} \tag{16}$$

$$\text{Max}\left|T^{n+1}-T^{n}\right|\leq 10^{-7} \tag{17}$$

where the calculation is carried out over the entire system.

Streamlines and isotherms predicted for flows at $Ra = 10^5$ and different inclination angles are shown in Figures 2 and 3. As can be seen from the figures of streamline plots, the liquid near the hot wall is heated and goes up due to the buoyancy effect before it hits the corner with the perfectly conducting walls and spread to a wide top wall. Then as it is cooled by the cold wall, the liquid gets heavier and goes downwards to complete the cycle.

At low value of inclination angle $(\theta = 20^0)$, two small vortices are formed at the upper corner and lower corner of the enclosure indicates high magnitude of flow velocity near these regions. The presence of these two corner vortices compressed the central cell to form an elongated vortex. The isotherms show a good mixing occurring in the center and relatively small gradient indicating small value of the local Nusselt number along the differentially heated walls.

Further increment of inclination angle $(\theta = 40^0)$ leads to the size reduction of small corner vortices. At $\theta = 60^0$, the small corner vortices completely disappear and the central cell pointing towards the corners because high magnitude of gravity vector drag the outer vortex along the vertical walls of the enclosure. Denser isotherms lines can be seen from the figure indicates higher value of local and average Nusselt number compared to previous inclination angles. Further inclination of enclosure separates the main central vortex into two smaller vortices. As we increase the inclination angle, these two vortices grow in size indicates that some fluid from the hot or cold wall returns back to the same wall. For inclination angles of $\theta = 80^0$ to $\theta = 120^0$, the isotherms line are parallel to the perfectly conducting walls indicates that the main heat transfer mechanism is by convection. Denser isotherms lines can be seen near the bottom left and top right corners demonstrates high local Nusselt number near these regions. However, at high inclination angles $(\theta \geq 140^0)$, the isotherms lines are equally spaced indicates low averages Nusselt number in the system.

For Rayleigh number equals to 5×10^5 and low inclination angles, the central vortex is more rounded indicates equal magnitude of flow velocity near all four enclosure walls. At angle equals to 60^0, the central cells splits into two before the corner vortices disappear. The velocity boundary layer can be clearly seen for inclination angles of 80^0 and above. The isotherm patterns are similar to those for $Ra = 10^5$ at all angles. However, the thermal boundary layer are thicker indicating higher local and average Nusselt number along the cold and hot walls.

For the simulation at the highest Rayleigh number in the present study $(Ra = 10^6)$, the formation of corner vortices can be clearly seen at low value of inclination angles. At angle equals to 20^0, the complex structure of upper corner vortices indicates the instability of the flow in the system. This flow instability is confirmed when we were unable to obtain a steady solution even for a very high iteration number. The isotherms plots also display a complex thermal behavior and good mixing of temperature in the system. The flow becomes steady again when we increase the inclination angle to 60^0. The central vortex is separated into two smaller vortices and vertically elongated shaped indicates relatively high value of flow velocity near the differentially heated walls. Most of the isotherms lines becomes parallel to the perfectly

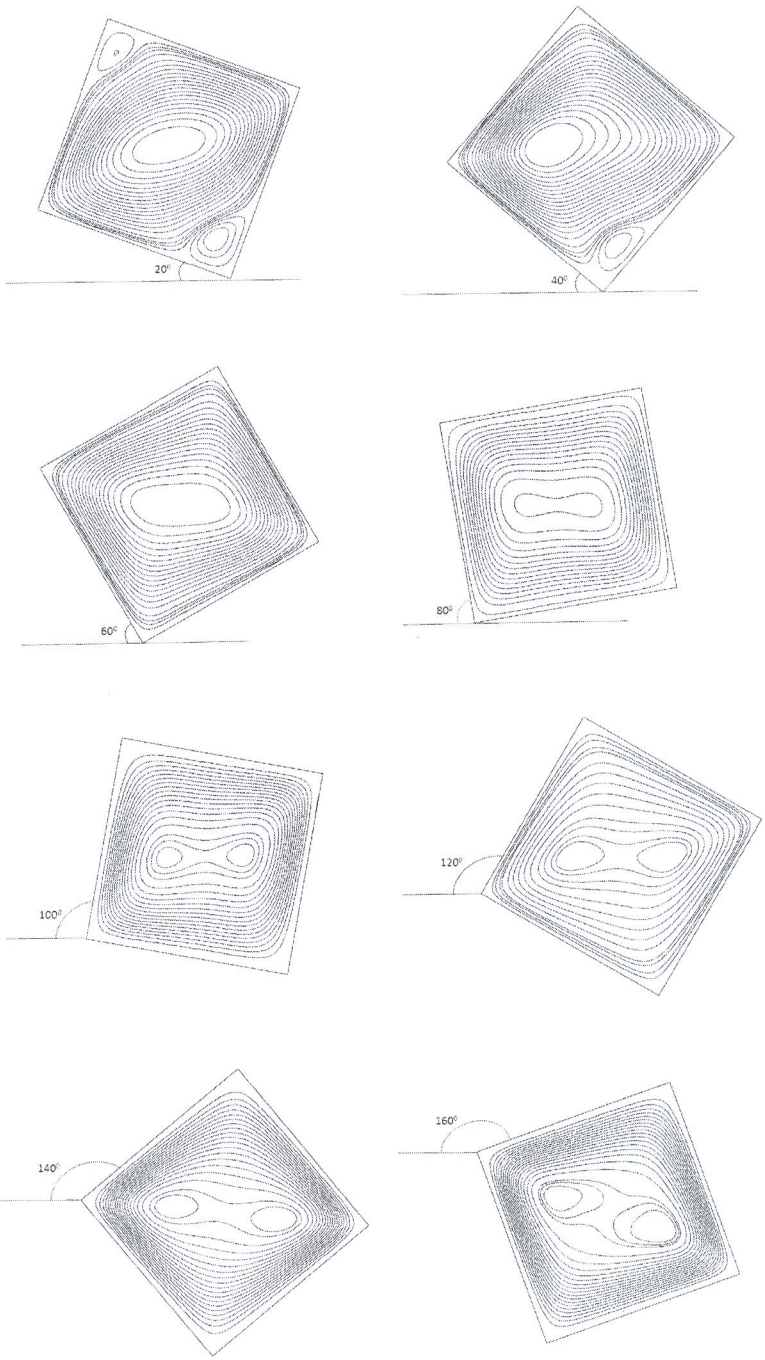

Figure 2. Streamlines plots at $Ra = 10^5$

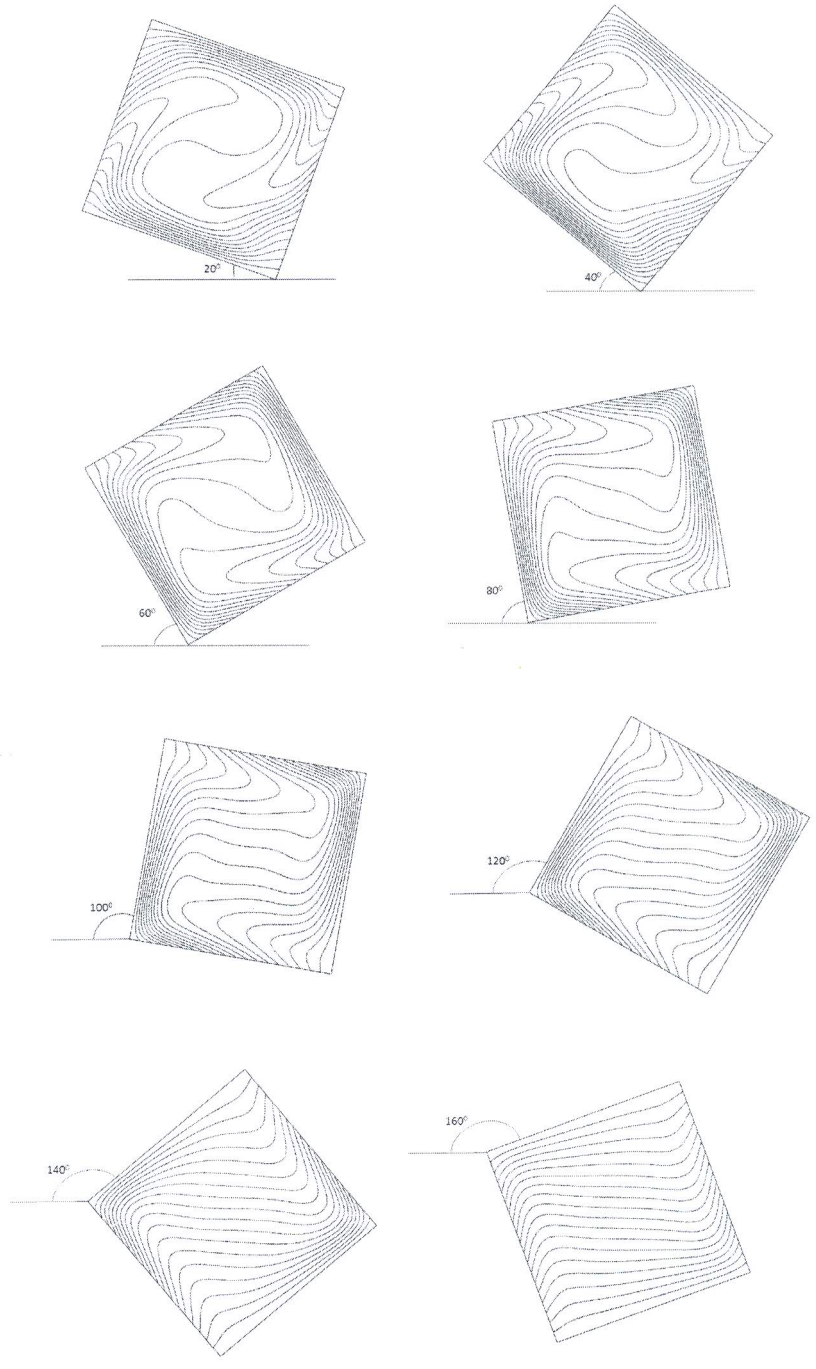

Figure 3. Isotherms plots at $Ra = 10^5$

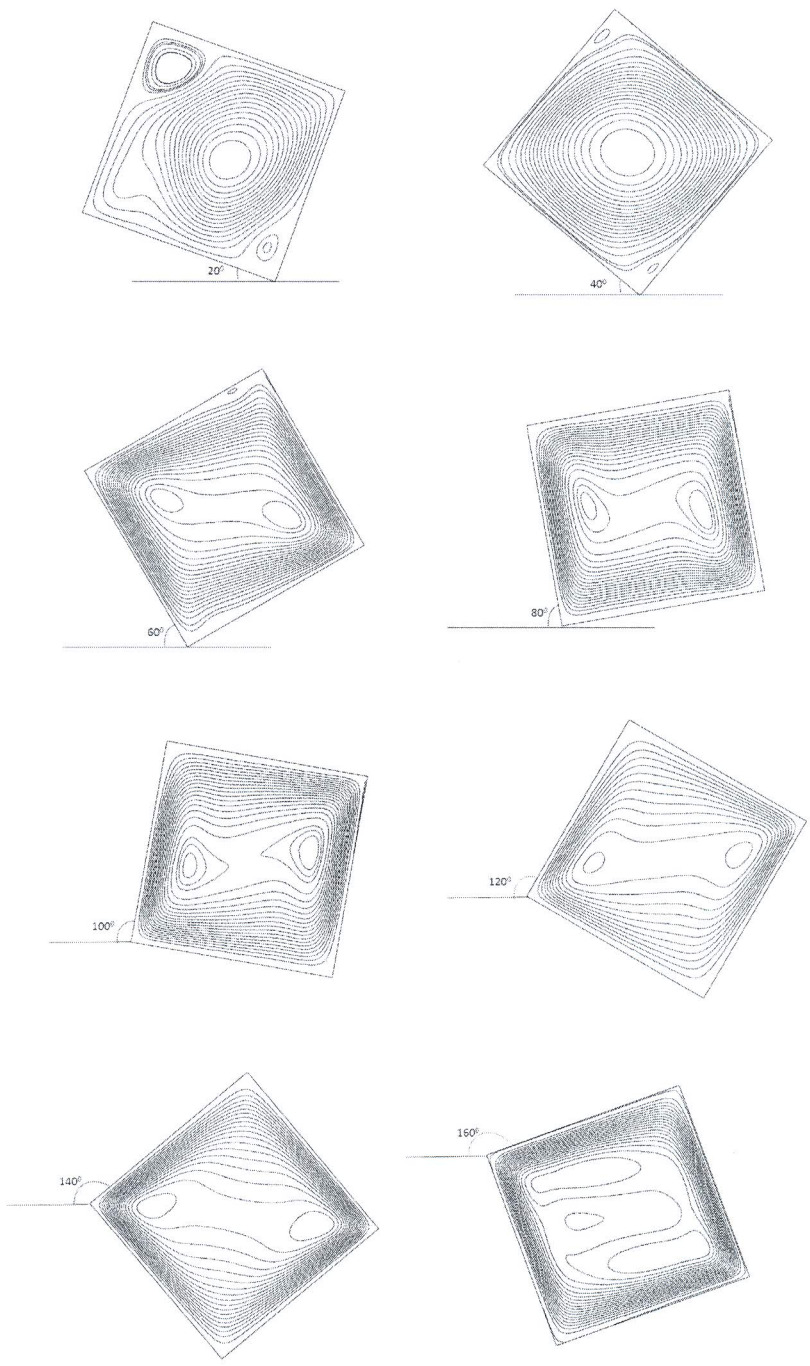

Figure 4. Streamlines plots at $Ra = 5 \times 10^5$.

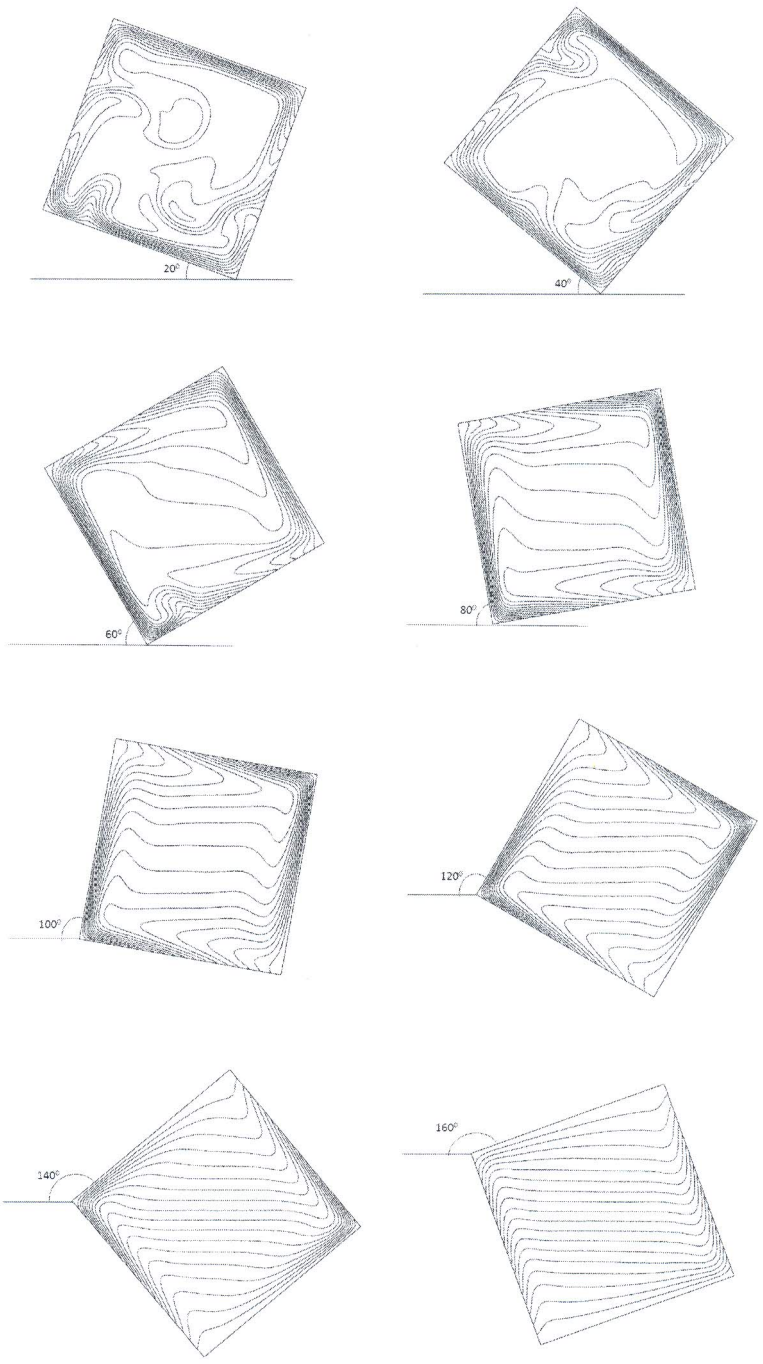

Figure 7. Isotherms plots at $Ra = 10^6$

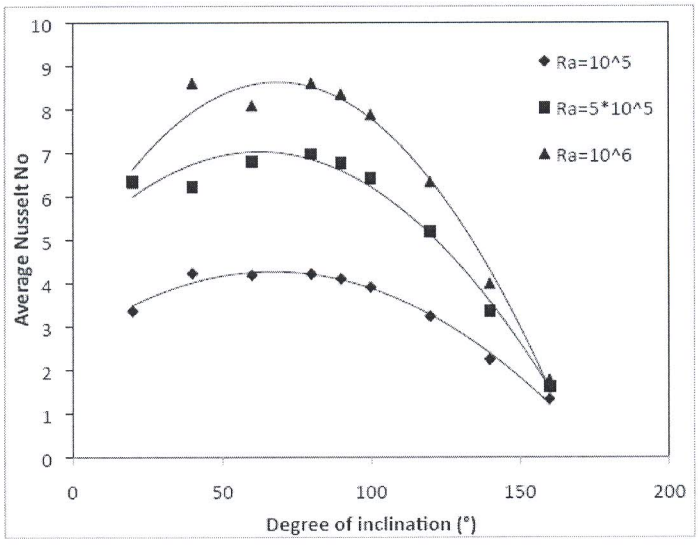

Figure 8. Effect of inclination angle on average Nusselt number.

conducting walls indicates the convection type dominates the heat transfer mechanism in the system.

For $\theta > 80^0$, the central vortex is stretched from corner to corner of the enclosure and perpendicular to the gravitational vector, developed denser streamlines near these corners, indicating the position of maximum flow velocity for the current condition. On the other hand, similar features of isotherms to those at lower Ra are observed.

The effect of the inclination angle on the average Nusselt number is shown in Figure 8 for all values of Rayleigh numbers. One common characteristic which can be drawn from the figure; the Nusselt number increases with increasing the Rayleigh number. However, the computed Nusselt numbers are lower than those for the case of adiabatic types of boundary condition[4] because the heat is allowed to pass through the top and bottom walls. Interestingly, the minimum value of average Nusselt number is found converging to the same value and when the inclination angle approaching 180^0 for every Rayleigh number. On the other hand, the maximum value of average Nusselt number is determined at inclination angle between 60^0 to 80^0. These can be explained by analyzing the isotherms plots which demonstrating relatively denser lines near hot and cold walls leading to high temperature gradient near these regions. Lower value of average Nusselt number at lower inclination angle was due to the presence of small corner vortices which contributes smaller local heat transfer along the hot and cold walls.

For the computation at higher inclination angles, where the hot wall is close to the top position, the magnitude of the gravity vector is reduced results in low magnitude of flow velocity along the hot wall. Due to this reason, the heat transfer rates are small resulted from the reduction in the driving potential for free convection.

4. CONCLUSION

The free convection in an inclined cavity has been simulated using the mesoscale numerical scheme where the Navier Stokes equation was solved indirectly using the lattice Boltzmann method. The result of streamlines plots clearly depicting the flow pattern and vortex structure in the cavity. The primary vortex is transformed from a single cellular to a double cellular as the inclination angle increases. These demonstrate the lattice Boltzmann numerical scheme of passive-scalar thermal lattice Boltzmann model is a very efficient numerical method to study flow and heat transfer in a differentially heated inclined enclosure.

Acknowledgement

The authors would like to acknowledge Universiti Teknologi Malaysia and Malaysia government for supporting these research activities. These research were conducted under FRGS research grant, Vot. 78340.

REFERENCES

1. Davis DV. *International Journal for Numerical Methods in Fluids* 1983; **3**(3):249–264.
2. Nor Azwadi CS, Tanahashi T. *International Journal of Modern Physics B* 2008; **22**(22):3865–3876.
3. Tric E, Labrosse G, Betrouni M. *International Journal of Heat and Mass Transfer* 2000; **43**(21):4043–4056.
4. Rasoul J, Prinos P. *International Journal of Numerical Methods for Heat and Fluid Flow* 1997; **7**(5):438–478.
5. Hart JE. *Journal of Fluid Mechanics* 1971; **47**(3):547–576.
6. Ozoe H, Yamamoto K, Sagama H, Churchill SW. *International Journal of Heat Mass Transfer* 1974; **17**(10):1209–1217.
7. kuyper RA, Meer VD, Hoogendoorn CJ, Henkes RAW. *International Journal of Heat Mass Transfer* 1993; **36**(11):2899–2911.
8. Nor Azwadi CS, Mohd Fairus MY, Samion S. *Journal of Applied Sciences* 2010; **10**(4):331–336.
9. Nor Azwadi CS, Tanahashi T. *International Journal of Modern Physics B* 2007; **21**(1):87–96.
10. Nor Azwadi CS, Tanahashi T. *International Journal of Modern Physics B* 2008; **22**(22):3865–3876.
11. Onishi J, Chen Y, Ohashi H. *JSME International Journal Series B* 2001; **44**(1):53–62.
12. Jami M, Mezrhab A, Bouzidi M, Lallemand P. *Physica A* 2006; **368**(2):481–494.
13. He X, Shan S, Doolen G. *Journal of Computational Physics* 1998; **146**(1):282–300.
14. Bhatnagar PL, Gross EP, Krook M. *Physical Review* 1954; **70**(3):511–525.
15. Shi Y, Zhao TS, Guo ZL. *Physical Review E* 2004; **70**(6):066310/1–066310/10.
16. He X, Luo LS. *Journal of Statistical Physics* 1997; **88**(3):927–944.
17. Peng Y, Shu C, Chew YT. *Physical Review E* 2003; **68**(2):020671/1–20671/8.

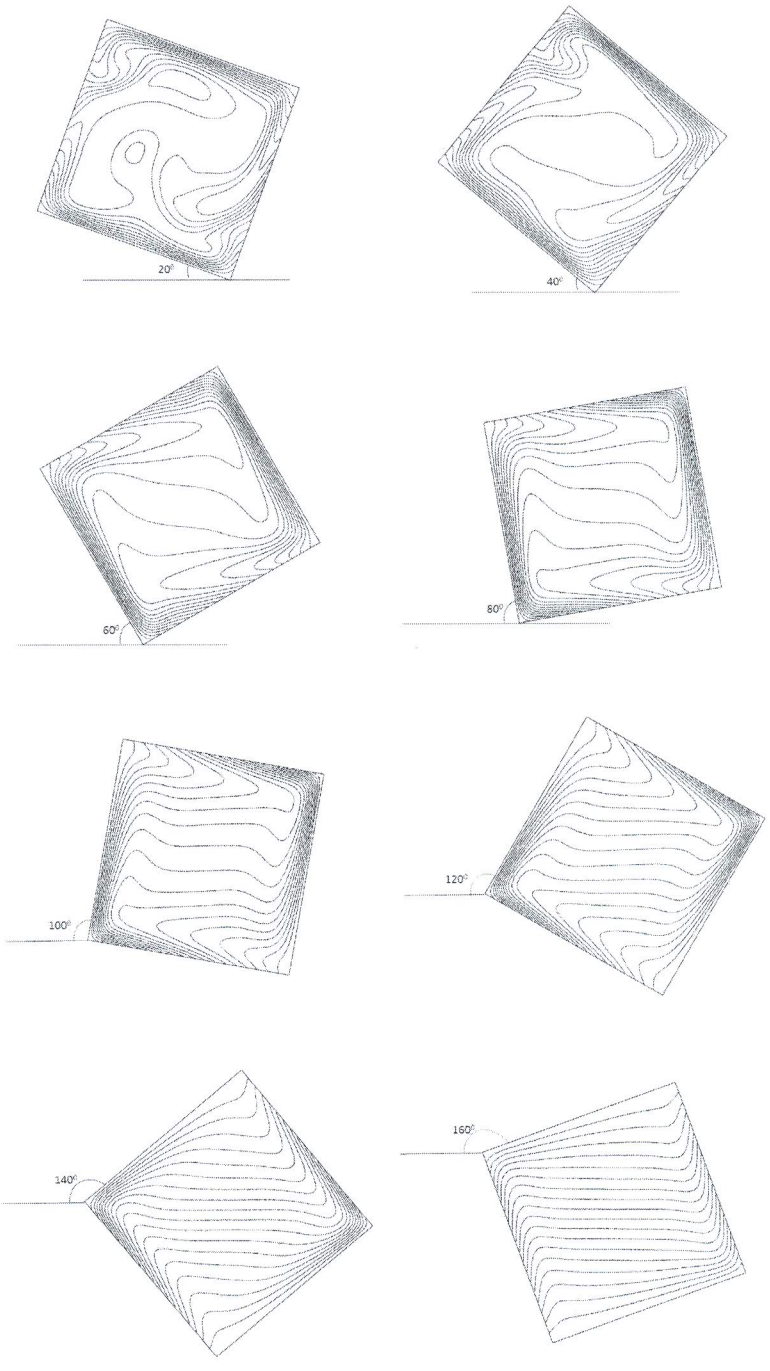

Figure 5. Isotherms plots at $Ra = 5 \times 10^5$

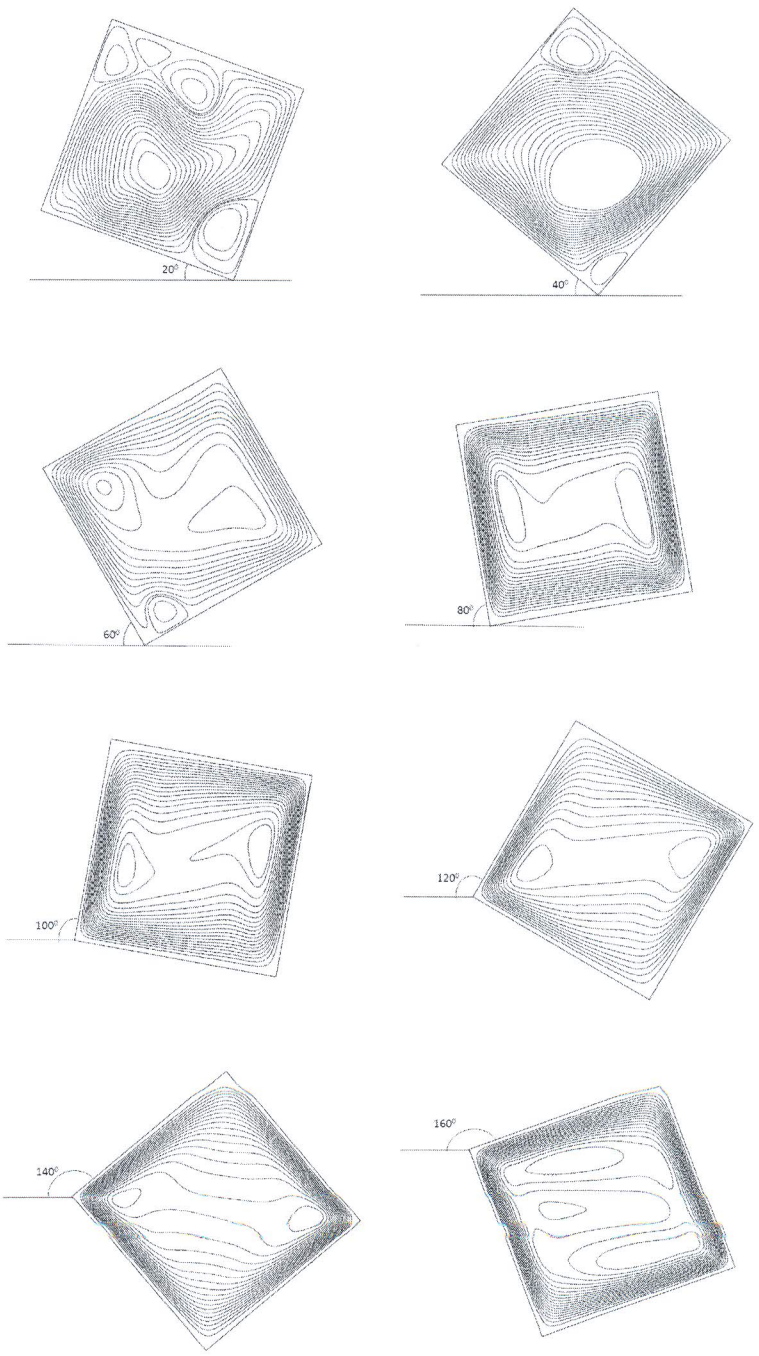

Figure 6. Streamlines plots at $Ra = 10^6$